

# Boosting the Transferability of Adversarial Attacks with Global Momentum Initialization

Jiafeng Wang<sup>1,2</sup> Zhaoyu Chen<sup>3</sup> Kaixun Jiang<sup>3</sup> Dingkan Yang<sup>3</sup>  
Lingyi Hong<sup>1,2</sup> Pinxue Guo<sup>3</sup> Haijing Guo<sup>1,2</sup> Wenqiang Zhang<sup>1,2,3</sup>

<sup>1</sup> School of Computer Science, Fudan University

<sup>2</sup> Shanghai Key Laboratory of Intelligent Information Processing

<sup>3</sup> Academy for Engineering and Technology, Fudan University

## Abstract

Deep neural networks are vulnerable to adversarial examples, which attach human invisible perturbations to benign inputs. Simultaneously, adversarial examples exhibit transferability under different models, which makes practical black-box attacks feasible. However, existing methods are still incapable of achieving desired transfer attack performance. In this work, from the perspective of gradient optimization and consistency, we analyze and discover the gradient elimination phenomenon as well as the local momentum optimum dilemma. To tackle these issues, we propose Global Momentum Initialization (GI) to suppress gradient elimination and help search for the global optimum. Specifically, we perform gradient pre-convergence before the attack and carry out a global search during the pre-convergence stage. Our method can be easily combined with almost all existing transfer methods, and we improve the success rate of transfer attacks significantly by an average of 6.4% under various advanced defense mechanisms compared to state-of-the-art methods. Eventually, we achieve an attack success rate of 95.4%, fully illustrating the insecurity of existing defense mechanisms. Code is available at <https://github.com/Omenzychen/Global-Momentum-Initialization>.

## 1. Introduction

Deep neural networks have shown superior performance in various tasks [1, 13, 14, 16, 17, 21, 25, 30–32, 43, 50–55], but they still exhibit high vulnerability to adversarial examples [3–6, 11, 19, 20, 23, 28, 41, 46, 56, 57], which make the model lose original performance by adding some imperceptible human perturbations. In addition, adversarial examples also exhibit transferability across models [18, 36, 37], i.e., adversarial examples generated by surrogate models can fool other models, making it possible to perform prac-

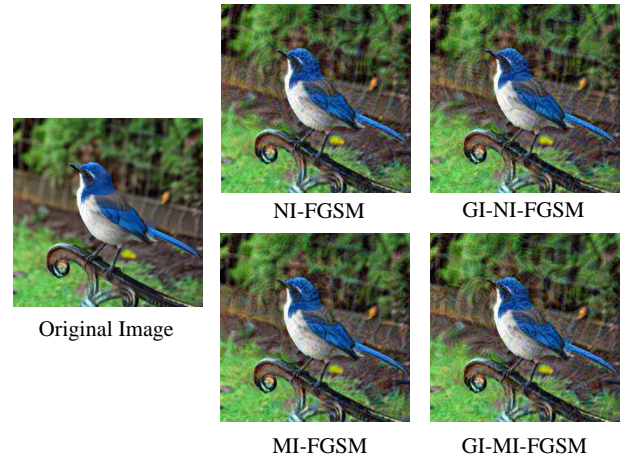


Figure 1. Adversarial examples are generated using the Inc-v3 model under NI-FGSM, MI-FGSM, and a combination of our method respectively. Subject to the constraint of a maximum perturbation limit at 16, we generate adversarial examples with approximate visualisation but achieve higher attack success rates.

tical black-box attacks [24]. Hence, further understanding the generation of adversarial examples with high transferability is of vital essence to improve model robustness.

Among the existing attack methods, the white-box attack strategy guarantees excellent attack performance by directly obtaining information about the target model, but struggles to achieve high transfer attack performance, especially for models with defense mechanisms. To tackle this challenge, a series of methods have also been proposed to improve transferability for more practical black-box attacks. These methods can be mainly divided into three perspectives: gradient optimization [8, 27, 44], data augmentation [9, 45, 48], and model integration [29]. In most cases, these methods can be integrated to obtain better attack performance.

Considering the aforementioned three attack perspectives, gradient optimization methods tend to be the most commonly used strategy given the availability of specific

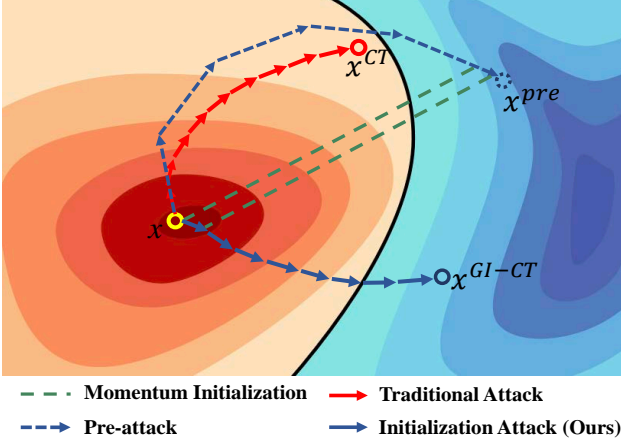


Figure 2. Visualisation of the attack process. Here CT represents the combination of three input transformation methods: DIM [48], TIM [9], SIM [27].  $x$  represents the original data point and  $x^{CT}$  represents the adversarial example obtained under original CT-FGSM.  $x^{pre}$  and  $x^{GI-CT}$  represent the example points pre-attacked and using global momentum initialization. Our method suppresses gradient elimination thus helps the gradients to be more consistent so as to successfully cross the decision boundary.

information about the surrogate model. From the standpoint of optimization, MI-FGSM [8], as one of the most important baselines, achieves higher attack consistency by introducing momentum to make the attack cumulative in the previous direction to help the attack direction out of the local optimum. Given that most of the existing optimization methods such as NI-FGSM [27], VT [44] are improved based on the momentum of MI-FGSM, so we mainly focus our analysis around momentum, phenomena of which remain prevalent in other optimization methods. Although momentum can improve the effectiveness of attacks, we discover the **gradient elimination** phenomenon still exists during the forward attack process, i.e., there is lower consistency for the forward unconverged gradients compared to the backward gradients, which may inhibit the transferability. Simultaneously, in the context of traditional iterative attacks, small step size of each iteration restricts the generated adversarial examples to be optimized within a very limited data distribution, which results in the attacks being more likely to fall into local optimum. Besides, a direct scaling of the step size may cause attack easily falling into overfitting. Please see **Supplementary Material 1** for more details.

To address the above issues, We first verify the potential relationship between gradient consistency and attack performance. Then, we propose global momentum initialization to suppress gradient elimination and locate better global optimum over a larger data distribution during pre-convergence. Concretely, we perform gradient pre-convergence in advance of the attack process to accelerate

momentum convergence, thus suppressing gradient elimination and employ global search in the pre-convergence phase to help the initial momentum converge at a more effective direction. The generated adversarial examples under different methods are shown in Figure 1. We visualise the attack process in Figure 2 for our method as well as the conventional method. The resulting experimental results show that even with various advanced defense mechanisms, our method can significantly improve the attack success rate by 6.4% compared to state-of-the-art method, and can eventually achieve an attack success rate of 95.4% on average. In summary, the main contributions are as follows:

- We investigate the reason why momentum can boost transferability in the perspective of gradient cosine similarity, and further identify the gradient elimination issue existing in momentum-based methods.
- We propose that Global momentum initialization (GI) helps the attack to find the global optimum within a larger data distribution while suppressing gradient elimination and thereby obtaining better attack performance.
- Our method can be easily combined with any existing gradient-based attack method. Empirical experiments show that our method can significantly outperform existing state-of-the-art methods under various attack settings.

## 2. Related Work

In this section, we present some gradient-based attack methods. Details of the defense methods can be found in the **Supplementary Material 2**.

### 2.1. Gradient Optimization Attacks

**Fast Gradient Sign Method (FGSM)** [11]. FGSM generates an adversarial example for only one step with the aim of maximizing the loss function:

$$x^{adv} = x^{clean} + \epsilon \cdot \text{sign}(\nabla_x J(x^{clean}, y)),$$

where  $\text{sign}(\cdot)$  represents the sign function.

**Iterative Fast Gradient Sign Method (I-FGSM)** [24]. In contrast to FGSM, I-FGSM divides one iteration into multiple small steps to obtain better attack directions:

$$x_{t+1}^{adv} = x_t^{adv} + \alpha \cdot \text{sign}(\nabla_x J(x_t^{adv}, y)),$$

where  $\alpha = \epsilon/T$  is the step size of each attack and  $T$  is the number of attack steps.

**Momentum Iterative Fast Gradient Sign Method (MI-FGSM)** [8]. Compared with white-box attacks, MI-FGSM integrates the momentum factor into attack to help the attack direction jump out of the local optimum:

$$g_{t+1} = \mu \cdot g_t + \frac{\nabla_x J(x_t^{adv}, y)}{\|\nabla_x J(x_t^{adv}, y)\|_1}, \quad (1)$$

$$x_{t+1}^{adv} = x_t^{adv} + \alpha \cdot \text{sign}(g_{t+1}),$$

where  $\mu$  is the decay factor and  $g_0 = 0$ .

**Nesterov Iterative Fast Gradient Sign Method (NI-FGSM)** [27]. NI-FGSM uses Nesterov’s accelerated gradient [35]  $x_t^{adv} + \alpha \cdot \mu \cdot g_t$  to replace  $x_t^{adv}$  in Eq. (1). This look-ahead process allows attack to move further away from the local optimum, resulting in better attack performance.

**Variance Tuning Method (VT)** [44]. VT performs gradient sampling in the domain of data points in each iteration, which in turn adjusts the direction of this gradient with variance tuning to form a more accurate attack direction.

## 2.2. Input Transformations Attacks

**Diverse Input Method (DIM)** [48]. DIM performs data augmentation using random scaling and padding operations with a certain probability to alleviate overfitting in adversarial attacks, which inspires one of the main perspectives of transferability enhancement.

**Translation-Invariant Method (TIM)** [9]. TIM applies convolution transformation of the Gaussian kernel  $W$  to the gradient information, which particularly boosts the attack performance against adversarial models.

$$x_{t+1}^{adv} = x_t^{adv} + \alpha \cdot \text{sign}(W \cdot \nabla_x J(D(x_t^{adv}), y)).$$

**Scale-Invariant Method (SIM)** [27]. SIM exploits the scaling invariance of the image and fuses the gradient information of different scaled images to improve the transferability under black box attack. The new optimization objective after scaling is:

$$\arg\max_{x_{adv}} \frac{1}{n} \sum_{i=0}^n J(S_i(x^{adv}), y),$$

where scaling factor  $S_i(x) = \frac{x}{2^i}$  and  $n$  is the scale number.

## 3. Methodology

Given the original image  $x^{clean}$  and the corresponding label  $y$ , the attacker has to find the perturbation  $\delta$  to generate adversarial examples  $x^{adv}$  to fool the model. To ensure the imperceptibility of the attack, following previous work, we apply the  $l_\infty$  norm, i.e., ensure that  $\|x^{clean} - x^{adv}\|_\infty \leq \epsilon$ . Assume that  $f(x^{adv})$  represents the output of the model with input  $x$  and the attack is to maximize the loss  $J(f(x^{adv}), y)$  (e.g. the cross-entropy loss or margin loss [2]), so the attack goal can be described as:

$$\arg\max_{x_{adv}} (J(f(x^{adv}), y)), \quad s.t. \|x^{clean} - x^{adv}\|_\infty \leq \epsilon.$$

### 3.1. Gradient Elimination

Among the existing gradient optimization methods, MI-FGSM, as a very important baseline, improves attack performance by introducing momentum to help accumulate

momentum sums of forward gradients, making the attack direction more consistent and preventing the attack from falling into a local optimum solution. Since most optimization-based methods improve on the momentum of MI-FGSM, our analysis revolves around MI-FGSM, and can be extended to other optimization methods (e.g. NI-FGSM). Here, we use **gradient consistency**, i.e., the degree of directional similarity during the attack to analyse the relationship between attack performance and attack direction exploration. We first develop a corollary of the numerical and theoretical relationship among different gradients.

Assuming that the gradient information obtained in the first round of attack is  $g_1$ , then the direction of the first round of attack is  $\text{sign}(g_1)$ , and the resulting difference of loss is:

$$\Delta J_1 = J(f(x + \alpha \cdot \text{sign}(g_1)), y) - J(f(x), y). \quad (2)$$

Further, from the Taylor expansion we can know:

$$f(x + \alpha \cdot \text{sign}(g_1)) = f(x) + \alpha \cdot \text{sign}(g_1) \cdot \frac{\partial f}{\partial x} + O(\alpha^2). \quad (3)$$

For the sake of simplicity, we denote  $\alpha \cdot \text{sign}(g_1) \cdot \frac{\partial f}{\partial x} + O(\alpha^2)$  as  $P(x)$ . Substituting Eq. (3) into Eq. (2), utilizing the Taylor expansion again to get:

$$\begin{aligned} J(f(x), y) &= J(f(x + \alpha \cdot \text{sign}(g_1)) - P(x), y) \\ &= J(f(x + \alpha \cdot \text{sign}(g_1)), y) \\ &\quad - T_1(x) \cdot \frac{\partial J}{\partial f} + O(P^2(x)). \end{aligned} \quad (4)$$

Combining Eq. (3) and Eq. (4), we can get:

$$\begin{aligned} \Delta J_1 &= P(x) \cdot \frac{\partial J}{\partial f} = (\alpha \cdot \text{sign}(g_1) \cdot \frac{\partial f}{\partial x} + O(\alpha^2)) \cdot \frac{\partial J}{\partial f} \\ &= \alpha \cdot \text{sign}(g_1) \cdot g_1 \approx \text{sign}(g_1) \cdot \text{sign}(g_1) > 0 \quad (g_1 \neq 0). \end{aligned} \quad (5)$$

Eq. 5 shows that when the first round gradient is attached to the input  $x$ , the loss change  $\Delta J_1 > 0$ , consistent with the fact that the loss turns larger during attack process. Similarly,  $\Delta J_n$  denotes that if the gradient of the  $n_{th}$  iteration is attached to input  $x$ , the difference of loss changes to  $\Delta J_n = \text{sign}(g_1) \cdot \text{sign}(g_n)$ . In this context, the input  $x$  can be an adversarial example derived from any iteration, so we can test the consistency between gradients of any two rounds to predict the change in loss. In conjunction with the optimization objective, a more effective attack is one that gains greater losses with other rounds. Therefore, to improve attack performance, we should ensure relatively higher gradient consistency.

Based on the above analysis, we further explore the consistency of gradients under momentum. As shown in Figure 3a, the cosimilarity between gradients that have not undergone momentum convergence is close to 0, meaning that there is a large randomness between the attack directions for

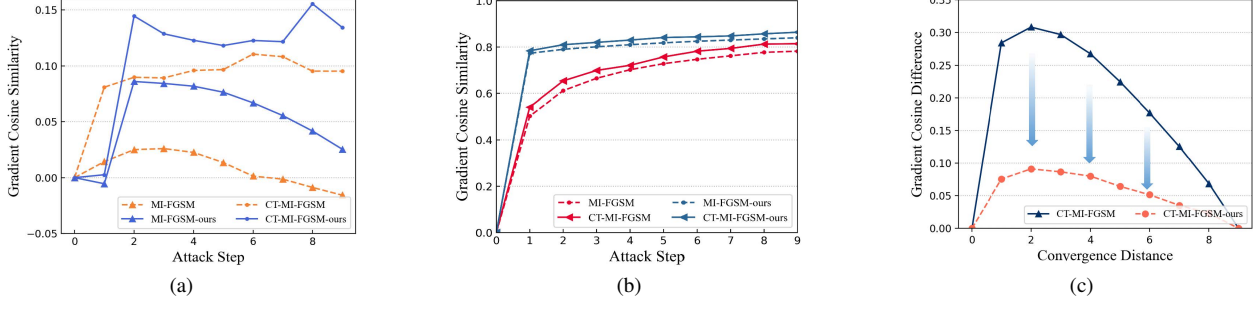


Figure 3. Analysis of gradient cosine similarity between iterative attacks. (a) represents the gradient cosine similarity before momentum accumulation; (b) represents the gradient cosine similarity between iterations after momentum accumulation; (c) shows the gradient similarity analysis between the first, last iteration after momentum processing and the gradients of the other iterations. The convergence distance represents the distance between iterations, for example, the convergence distance between 1<sup>st</sup> round and 9<sup>th</sup> round to 5<sup>th</sup> round is the same, and the gradient cosine difference represents the difference in gradient similarity under the same convergence distance, with a larger difference indicating a larger discrepancy in the direction of the forward and backward gradient attack of the original gradient.

---

**Algorithm 1: Framework of GI-MI-FGSM**


---

**Input:** A classifier  $f$  with fixed parameters  $\theta$  and loss function  $J$ , number of iterations  $T$ , maximum perturbation  $\epsilon$ , input images  $x$ , Pre-convergence Iterations  $P$ ; Global Search Factor  $S$

**Output:** An adversarial example  $x^{adv}$ ;

```

1  $g_0 = 0$ ;  $x_0^{adv} = x$ ;  $\alpha = \epsilon / T$ ;
2 for  $t = 0 \rightarrow P - 1$  do
3    $g_{t+1} = \mu \cdot g_t + \frac{\nabla_x J(x_t^{adv}, y)}{\|\nabla_x J(x_t^{adv}, y)\|_1}$ ;
4    $x_{t+1}^{adv} = \text{Clip}(x_t^{adv} + s \cdot \alpha \cdot \text{sign}(g_{t+1}))$ ;
5 end
6 Set global momentum initialization  $g_0 = g_P$ ;
7 for  $t = 0 \rightarrow T - 1$  do
8    $g_{t+1} = \mu \cdot g_t + \frac{\nabla_x J(x_t^{adv}, y)}{\|\nabla_x J(x_t^{adv}, y)\|_1}$ ;
9    $x_{t+1}^{adv} = \text{Clip}(x_t^{adv} + \alpha \cdot \text{sign}(g_{t+1}))$ ;
10 end
11  $x^{adv} = x_T^{adv}$ ;
12 return  $x^{adv}$ ;
```

---

different iteration rounds. On the other hand, Figure 3b illustrates the gradient consistency of different rounds during the attack after the momentum treatment, and it can be seen that after a few rounds of forward gradient convergence, the gradient consistency rapidly improves and reaches stability. This indicates that the momentum helps the attack gradients to find common directions, e.g. feature-based consistent attacks, thus improving the attack performance. Simultaneously, when combined with existing data enhancement methods CT, the attack can explore more generalised attack directions with higher attack consistency, further improving attack performance. The experimental results with CT are detailed in Section 4.3.

Furthermore, instead of focusing on the impact on attack direction generalizability brought by data augmentation, we analyse the impact of forward gradient convergence on attack performance from an optimization perspective. As Figure 3b depicts, we can see that although momentum can accelerate the gradient to reach consistency, there still exists a convergence process, which to a certain extent inhibits the attack performance improvement. We define this phenomenon where the forward gradient does not converge enough resulting in a less consistent attack direction as gradient elimination. To fully explore this phenomenon, we further probe the gradient consistency of the forward unconverged gradient as well as the backward converged gradient with other iterations, respectively. As shown in Figure 3c, with the same convergence distance guaranteed, the forward unconverged gradient is significantly less consistent with the other rounds compared to the backward converged gradient. This also suggests that the leap of the forward gradient towards the decision boundary is insufficient due to the lack of convergence, again confirming the phenomenon of gradient elimination.

### 3.2. Global Momentum Initialization

In this subsection, we first propose pre-convergence attack to solve the problem of gradient elimination in order to help the attack converge faster to form a better attack. Additionally, we use global search during the pre-convergence period to overcome the limitation that conventional iterative methods generate gradients within a small data distribution. Finally, we get our global gradient initialization method.

To cope with gradient elimination, we attempt to pre-converge the momentum before the formal iterative attack, which poses no actual effect of the attack on the image. Specifically, we first perform  $P$  rounds of momentum exploration, using the momentum after  $P$  iterations as the initialised momentum. By means of this pre-convergence, we



Model	Attack	Inc-v3	Inc-v4	IncRes-v2	Res-101	Inc-v3 <sub>ens3</sub>	Inc-v3 <sub>ens4</sub>	IncRes-v2 <sub>ens</sub>	Average
Inc-v3	MI-FGSM	<b>100.0*</b>	44.4	41.5	34.7	<b>14.5</b>	12.4	6.0	36.2
	GI-MI-FGSM	<b>100.0*</b>	<b>54.1</b>	<b>51.9</b>	<b>43.8</b>	14.3	<b>13.4</b>	<b>6.6</b>	<b>40.6</b>
	NI-FGSM	<b>100.0*</b>	52.1	49.9	42.6	<b>13.7</b>	<b>13.9</b>	6.0	39.7
	GI-NI-FGSM	<b>100.0*</b>	<b>58.7</b>	<b>56.0</b>	<b>47.5</b>	13.4	12.0	<b>6.8</b>	<b>42.1</b>
Inc-v4	MI-FGSM	56.3	99.7*	46.7	41.3	<b>16.4</b>	14.8	7.6	40.4
	GI-MI-FGSM	<b>68.6</b>	<b>100.0*</b>	<b>57.0</b>	<b>51.0</b>	16.1	<b>15.8</b>	<b>7.7</b>	<b>45.2</b>
	NI-FGSM	63.3	<b>100.0*</b>	51.1	45.9	15.1	14.4	7.0	42.4
	GI-NI-FGSM	<b>74.7</b>	<b>100.0*</b>	<b>62.4</b>	<b>53.3</b>	<b>16.8</b>	<b>16.2</b>	<b>8.1</b>	<b>47.4</b>
IncRes-v2	MI-FGSM	58.7	50.9	98.1*	45.1	21.6	17.2	11.5	43.3
	GI-MI-FGSM	<b>73.9</b>	<b>64.3</b>	<b>98.5*</b>	<b>57.2</b>	<b>23.0</b>	<b>17.7</b>	<b>12.3</b>	<b>49.6</b>
	NI-FGSM	61.6	54.5	99.1*	45.5	20.1	16.0	9.5	43.8
	GI-NI-FGSM	<b>77.1</b>	<b>68.3</b>	<b>99.5*</b>	<b>58.8</b>	<b>23.8</b>	<b>18.0</b>	<b>11.7</b>	<b>51.0</b>
Res-101	MI-FGSM	58.8	50.8	50.8	99.1*	24.3	<b>22.0</b>	<b>12.9</b>	45.5
	GI-MI-FGSM	<b>71.1</b>	<b>64.6</b>	<b>64.2</b>	<b>99.3*</b>	<b>26.2</b>	21.2	12.4	<b>51.3</b>
	NI-FGSM	64.3	59.4	55.9	99.4*	24.1	<b>21.2</b>	<b>12.3</b>	48.1
	GI-NI-FGSM	<b>74.7</b>	<b>68.6</b>	<b>65.9</b>	<b>99.5*</b>	<b>26.9</b>	21.1	12.0	<b>52.7</b>

Table 1. Attack success rates (%) of seven models using optimization method merely. The adversarial examples are crafted by Inc-v3, Inc-v4, IncRes-v2, Res-101 respectively. \* indicates the white-box attack setting.

are able to substantially suppress the forward gradient elimination phenomenon. As shown in Figure 3b and 3c, the consistency of the forward gradient after pre-convergence is substantially improved, and the difference in gradient consistency between the forward and backward gradients and other rounds of gradients is significantly reduced, both of which indicate the pre-converged gradients can accelerate convergence and obviously improve the attack performance.

Moreover, the traditional iterative attack sets a small step size, which leaves the generated images after each round of the attack in a relatively similar data distribution. This prevents the attack from finding decision boundary over a larger data distribution, leading to a tendency to fall into local optimal solutions. Gao et al. [10] propose to scale up the step size, but this approach will have a direct impact on the images and easily cause overfitting of the attack. To address this issue, we add a global search factor to the pre-convergence process, i.e., we amplify the exploration step size during pre-convergence to help form a more global direction of initialised momentum. Namely, we perform gradient pre-convergence by:

$$g_{t+1} = \mu \cdot g_t + \frac{\nabla_x J(x_t^{adv}, y)}{\|\nabla_x J(x_t^{adv}, y)\|_1},$$

$$x_{t+1}^{adv} = \text{Clip}(x_t^{adv} + S \cdot \alpha \cdot \text{sign}(g_{t+1})),$$

where  $S$  represents our global search factor and  $\text{Clip}(\cdot)$  operation ensures the  $l_\infty$  constraint. The procedure of the attack based on global momentum initialization can be summarised as Algorithm 1.

To further demonstrate that global momentum initialization can help suppress gradient elimination, we visualise the attack process in Figure 2 for our method as well as the

conventional method. Since the direction of the attack gets progressively closer to the decision boundary during the optimization, traditional iterative methods may easily suffer from gradient elimination in the forward unconverged attack, i.e., they can only get closer to the decision boundary by a minor distance. For this reason, with the exploration of pre-attack and global momentum initialization, the attack strategy can search for a better attack direction in advance and ensure the consistency of the attack process to successfully cross the decision boundary.

## 4. Experiment

### 4.1. Experiment Setup

**Dataset.** Followed by NIPS’17 Competition [24], we randomly select 1,000 images from the ILSVRC 2012 validation set [38], correctly classified and belonging to different categories as our original inputs.

**Models.** We consider four normally trained models, including Inception-v3 (Inc-v3) [40], Inception-v4 (Inc-v4) [39], Inception-Resnet-v2 (IncRes-v2) and Resnet-101 (Res-101) [15] as well as three adversarially trained models, namely ens3-adv-Inception-v3 (Inc-v3<sub>ens3</sub>), ens4-adv-Inception-v3 (Inc-v3<sub>ens4</sub>) and ens-adv-Inception-ResNet-v2 (IncRes-v2<sub>ens</sub>) [42]. In addition, we adopt nine advanced defense methods to test the attack performance, e.g. HGD [26], R&P [47], NIPS-r3<sup>1</sup>, JPEG [12], FD [33], ComDefend [22], NRP [34], RS [7], Bit-Red [49].

**Baselines.** For optimization methods, we regard MI-FGSM and NI-FGSM as our baselines. Simultaneously, for

<sup>1</sup><https://github.com/anlthms/nips-2017/tree/master/mmd>

Model	Attack	Inc-v3	Inc-v4	IncRes-v2	Res-101	Inc-v3 <sub>ens3</sub>	Inc-v3 <sub>ens4</sub>	IncRes-v2 <sub>ens</sub>	Average
Inc-v3	NI-CT-FGSM	99.5*	84.5	79.0	72.9	57.2	54.8	40.3	69.7
	GI-NI-CT-FGSM	<b>99.8*</b>	<b>93.7</b>	<b>91.0</b>	<b>87.1</b>	<b>70.1</b>	<b>65.9</b>	<b>50.0</b>	<b>79.7</b>
	VNI-CT-FGSM	99.0*	90.1	87.6	84.6	78.6	76.5	66.0	83.2
	GI-VNI-CT-FGSM	<b>99.3*</b>	<b>94.5</b>	<b>92.7</b>	<b>89.7</b>	<b>85.1</b>	<b>83.3</b>	<b>72.9</b>	<b>88.2</b>
	MI-CT-FGSM	98.7*	85.4	80.6	76.0	64.1	62.1	45.2	73.2
	GI-MI-CT-FGSM	<b>99.4*</b>	<b>93.4</b>	<b>91.8</b>	<b>87.6</b>	<b>74.9</b>	<b>68.8</b>	<b>53.5</b>	<b>81.3</b>
	VMI-CT-FGSM	99.0*	88.5	85.7	82.4	77.3	75.9	62.8	81.7
	GI-VMI-CT-FGSM	<b>99.5*</b>	<b>97.1</b>	<b>95.9</b>	<b>92.8</b>	<b>88.0</b>	<b>86.5</b>	<b>74.9</b>	<b>90.7</b>
Inc-v4	NI-CT-FGSM	87.8	99.4*	82.5	75.9	65.8	62.6	51.3	75.0
	GI-NI-CT-FGSM	<b>95.0</b>	<b>99.5*</b>	<b>93.4</b>	<b>87.3</b>	<b>76.7</b>	<b>71.2</b>	<b>59.5</b>	<b>83.2</b>
	VNI-CT-FGSM	92.3	99.7*	89.2	84.9	79.9	77.1	70.5	84.8
	GI-VNI-CT-FGSM	<b>97.6</b>	<b>99.7*</b>	<b>92.6</b>	<b>90.7</b>	<b>88.1</b>	<b>86.2</b>	<b>79.8</b>	<b>90.7</b>
	MI-CT-FGSM	87.2	98.6*	83.3	78.3	72.2	67.2	57.3	77.7
	GI-MI-CT-FGSM	<b>94.5</b>	<b>99.5*</b>	<b>93.2</b>	<b>87.8</b>	<b>77.3</b>	<b>73.8</b>	<b>61.2</b>	<b>83.9</b>
	VMI-CT-FGSM	89.7	98.8*	86.3	82.0	78.1	76.2	67.5	82.7
	GI-VMI-CT-FGSM	<b>97.0</b>	<b>99.8*</b>	<b>95.5</b>	<b>91.7</b>	<b>88.3</b>	<b>86.8</b>	<b>79.4</b>	<b>91.2</b>
IncRes-v2	NI-CT-FGSM	90.2	87.0	99.4*	83.2	75.0	68.9	65.1	81.3
	GI-NI-CT-FGSM	<b>96.0</b>	<b>95.3</b>	<b>99.4*</b>	<b>92.0</b>	<b>84.3</b>	<b>80.7</b>	<b>75.7</b>	<b>89.1</b>
	VNI-CT-FGSM	92.9	90.6	99.0*	88.2	85.2	82.5	81.8	88.6
	GI-VNI-CT-FGSM	<b>96.3</b>	<b>97.3</b>	<b>99.3*</b>	<b>95.4</b>	<b>94.4</b>	<b>91.6</b>	<b>91.0</b>	<b>95.0</b>
	MI-CT-FGSM	88.0	85.5	97.5*	81.6	76.0	71.5	70.2	81.5
	GI-MI-CT-FGSM	<b>95.3</b>	<b>94.7</b>	<b>99.0*</b>	<b>91.4</b>	<b>85.6</b>	<b>82.1</b>	<b>78.4</b>	<b>89.5</b>
	VMI-CT-FGSM	88.9	87.0	97.0*	85.0	83.4	80.5	79.4	85.9
	GI-VMI-CT-FGSM	<b>96.9</b>	<b>96.3</b>	<b>99.4*</b>	<b>94.4</b>	<b>92.6</b>	<b>91.0</b>	<b>89.9</b>	<b>94.4</b>
Res-101	NI-CT-FGSM	86.1	82.2	83.3	98.5*	70.0	68.5	54.6	77.6
	GI-NI-CT-FGSM	<b>94.9</b>	<b>92.7</b>	<b>93.2</b>	<b>99.3*</b>	<b>83.4</b>	<b>78.3</b>	<b>68.7</b>	<b>87.2</b>
	VNI-CT-FGSM	90.7	85.5	87.2	99.1*	82.6	79.7	73.3	85.4
	GI-VNI-CT-FGSM	<b>96.3</b>	<b>95.6</b>	<b>95.5</b>	<b>99.4*</b>	<b>92.4</b>	<b>90.5</b>	<b>85.5</b>	<b>93.6</b>
	MI-CT-FGSM	86.5	81.8	83.2	98.9*	77.0	72.3	61.9	80.2
	GI-MI-CT-FGSM	<b>94.0</b>	<b>92.2</b>	<b>91.8</b>	<b>99.3*</b>	<b>83.9</b>	<b>80.4</b>	<b>70.0</b>	<b>87.4</b>
	VMI-CT-FGSM	86.9	84.2	86.4	98.6*	81.0	78.6	71.6	83.9
	GI-VMI-CT-FGSM	<b>95.8</b>	<b>95.3</b>	<b>94.9</b>	<b>99.3*</b>	<b>92.3</b>	<b>89.8</b>	<b>85.2</b>	<b>93.2</b>

Table 2. Attack success rates (%) of seven black models using both optimization methods and transformation methods. The adversarial examples are crafted by Inc-v3, Inc-v4, IncRes-v2, Res-101 respectively. \* indicates the white box attack setting.

data augmentation methods, we consider DIM, TIM, SIM, CT, i.e., the integrated version of the former three methods, and the VT as the baselines. When combining our method with present optimization and input transformation methods, we denote final methods as GI-VM(N)I-CT-FGSM, GI-M(N)I-CT-FGSM and GI-M(N)I-FGSM, respectively.

**Hyper-parameters.** We follow the attack settings of [44] and set the maximum perturbation  $\epsilon$  to 16, the number of iteration rounds  $T$  to 10 and the iteration step size  $\alpha$  to 1.6. We set decay factor  $\mu$  to 1 for MI-FGSM and NI-FGSM. As for input transformation methods, we set transformation probability to 0.5 for DIM. We adopt  $7 \times 7$  Gaussian kernel for TIM and the scale number for SIM equals to 5. For our method, we set pre-convergence iterations  $P$  to 5 and global search factor  $S$  to 10.

## 4.2. Attack with Optimization Methods

Initially, we evaluate the performance of our method with the optimization method only, i.e., we combine our method to NI-FGSM and MI-FGSM respectively without considering the input transformation methods. Here we use the attack success rate, the proportion of images misclassified by the attack model as our metric. During the attack we use four normally trained models as surrogate models to generate adversarial examples iteratively and then transfer them to all models, results of which are shown in Table 1.

According to the results, we can see that for the four normally trained models, our method improves the black-box attack transferability by a large margin while improving the white-box performance as well, e.g., for the adversarial examples generated by IncRes-v2 and transferred to Inc-v3, the attack success rate increases from 58.7% and 61.6% to 73.9% and 77.1%, respectively. However, at the same time, we also notice that the improvement for the ad-

Attack	Inc-v3	Inc-v4	Inc-Res-v2	Res-101	Inc-v3 <sub>ens3</sub>	Inc-v3 <sub>ens4</sub>	IncRes-v2 <sub>ens</sub>	Average
MI-CT-FGSM	99.4*	99.0*	97.6*	99.7*	91.3	90.1	86.6	94.8
GI-MI-CT-FGSM	<b>100.0*</b>	<b>99.9*</b>	<b>99.8*</b>	<b>100.0*</b>	<b>98.0</b>	<b>97.2</b>	<b>95.0</b>	<b>98.6</b>
NI-CT-FGSM	<b>100.0*</b>	<b>100.0*</b>	99.8*	<b>100.0*</b>	91.8	89.1	84.5	95.0
GI-NI-CT-FGSM	<b>100.0*</b>	99.9*	<b>100.0*</b>	<b>100.0*</b>	<b>98.2</b>	<b>97.4</b>	<b>95.4</b>	<b>98.7</b>
VMI-CT-FGSM	99.7*	99.1*	98.6*	<b>100.0*</b>	93.2	92.3	90.4	96.2
GI-VMI-CT-FGSM	<b>100.0*</b>	<b>100.0*</b>	<b>100.0*</b>	<b>100.0*</b>	<b>98.9</b>	<b>98.6</b>	<b>97.4</b>	<b>99.3</b>
VNI-CT-FGSM	99.7*	99.6*	99.2*	99.9*	94.9	93.8	92.0	97.0
GI-VNI-CT-FGSM	<b>100.0*</b>	<b>100.0*</b>	<b>100.0*</b>	<b>100.0*</b>	<b>98.9</b>	<b>98.5</b>	<b>97.6</b>	<b>99.3</b>

Table 3. Attack success rates (%) of seven models using both optimization methods and input transformation methods. The adversarial examples are crafted by the ensemble of Inc-v3, Inc-v4, IncRes-v2, Res-101 models. \* indicates the white box attack setting.

Attack	HGD	R&P	NIPS-r3	JPEG	FD	ComDefend	NRP	RS	Bit-Red	Average
MI-CT-FGSM	90.8	88.1	87.6	92.1	88.5	90.4	76.4	69.3	76.4	84.4
GI-MI-CT-FGSM	<b>97.0</b>	<b>95.2</b>	<b>95.8</b>	<b>98.2</b>	<b>95.7</b>	<b>98.1</b>	<b>83.1</b>	<b>78.7</b>	<b>84.3</b>	<b>91.8</b>
NI-CT-FGSM	90.7	86.6	86.5	92.8	89.7	91.3	69.8	64.2	72.2	82.6
GI-NI-CT-FGSM	<b>97.6</b>	<b>95.7</b>	<b>95.9</b>	<b>98.3</b>	<b>95.9</b>	<b>97.3</b>	<b>81.4</b>	<b>78.8</b>	<b>83.8</b>	<b>91.6</b>
VMI-CT-FGSM	92.8	90.4	89.9	93.4	91.2	92.2	83.3	76.9	80.4	87.8
GI-VMI-CT-FGSM	<b>98.5</b>	<b>97.7</b>	<b>97.4</b>	<b>99.0</b>	<b>96.6</b>	<b>98.3</b>	<b>90.3</b>	<b>86.8</b>	<b>89.9</b>	<b>94.9</b>
VNI-CT-FGSM	94.1	92.4	91.6	95.1	92.2	92.3	84.5	77.4	81.4	89.0
GI-VNI-CT-FGSM	<b>98.9</b>	<b>98.1</b>	<b>98.0</b>	<b>99.1</b>	<b>97.8</b>	<b>98.2</b>	<b>90.8</b>	<b>87.2</b>	<b>90.5</b>	<b>95.4</b>

Table 4. Attack success rates (%) of nine advanced defense methods using both optimization methods and transformation methods. The adversarial examples are crafted by the ensemble of Inc-v3, Inc-v4, IncRes-v2, Res-101 models.

versarial trained models is not as significant as that for the normally trained models. We attribute this to the inherent low transferability of the adversarially trained model, which results in the original attack direction not being able to explore a better global optimal direction even after better optimization. This phenomenon will be eliminated when combined with the input transformation methods, details of which are available in Section 4.3.

### 4.3. Attack with Input Transformation

Further, we verify the performance of GI with both the optimization and input transformation methods. We integrate it into several state-of-the-art methods under DIM, SIM, and TIM respectively to test its performance. The results are shown in the **Supplementary Material 3**, and it can be seen that combining our methods can lead to a significant increase in the success rate of the attack.

Moreover, we follow the experimental setup CTM in [27] and then combine them with the gradient optimization methods: MI-FGSM, NI-FGSM and VT respectively to test the performance. It is important to mention here that the VT brings non-negligible time and space cost in terms of attack performance, so in order to make a fair comparison, we test attack performance under both M(N)I-CT-FGSM and VM(N)I-CT-FGSM. The final results are shown in the Table 2. Overall, under M(N)I-CT-FGSM condition, our method can further improve the attack success rate by 8.1% in average, and the attack performance achieve that of the

previous state-of-the-art method VM(N)I-CT-FGSM while obtaining a significant reduction in attack time and space costs. In particular, the final method, GI-M(N)I-VT-FGSM, can achieve an average attack success rate of 88.2% ~ 95%, which exceeds previous state-of-the-art method VM(N)I-CT-FGSM by 7.6% in average.

### 4.4. Attack with Ensemble Models

The previous two subsections verify the generality as well as the high performance of our global momentum initialization approach. Besides, Liu et al. [29] have shown that the adversarial examples generated with the ensemble model are more transferable, therefore, in this subsection, we continue to verify the performance under the integrated attack, and the results are shown in Table 3. From the results, we see that our method significantly improves the effectiveness of the black-box attack and also improves the performance of the white-box attack to some extent under both CT and VT. It is worth mentioning that with the ensemble model method, our attack success rate reaches more than 98.6% on average, which means that we can basically achieve the performance of white-box attack. And under white-box attack setting, the attack success rate can reach 100% at most circumstances.

### 4.5. Evaluation on Advanced Defense Methods

To further investigate the performance of our approach under advanced defense methods, we selected several of-

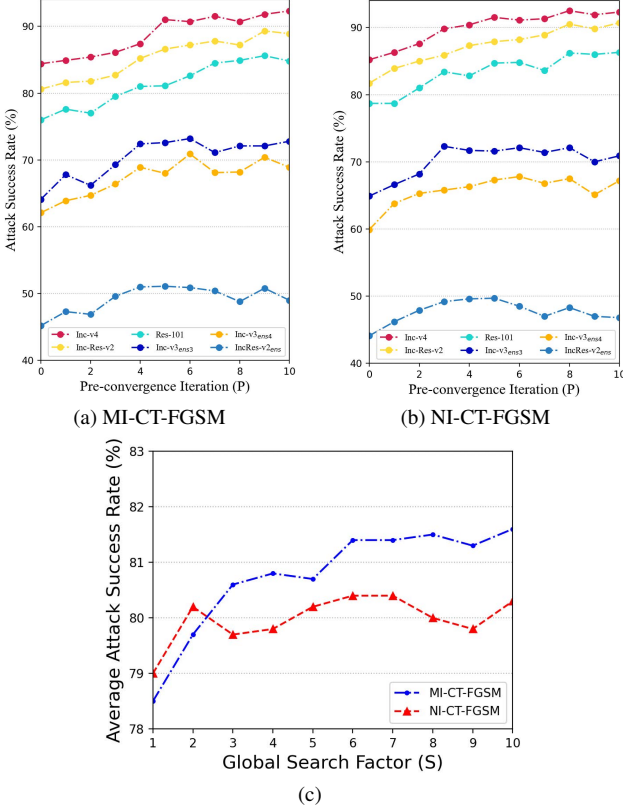


Figure 4. Ablation experiments on pre-convergence and global search factors. (a) and (b) represent attack success rate for six black box models using different pre-convergence iterations. (c) represents the average attack success rate of six models with different global search factors. All adversarial examples are generated by Inc-v3 under MI-CT-FGSM and NI-CT-FGSM respectively.

ficial baselines from the NIPS 2017 competition [24] for testing, such as HGD [26], R&P [47], NIPS-r3, along with several classical methods for adversarial defense, such as JPEG [12], FD [33], ComDefend [22], NRP [34], RS [7], Bit-Red [49], to further test the performance of attacks under defense conditions. Here we test the attack performance with the integrated model and the single model (Inc-v3) respectively. The attack results for the integrated model are shown in Table 4, and the results for the single model can be found in the **Supplementary Material 4**.

The results are impressive in that our attack method achieves an average attack success rate of 91.6%  $\sim$  95.4%, outperforming the previous VM(N)I-CT-FGSM method by 6.4%  $\sim$  9.0%, which also indicates the vulnerability and fragility of the existing defense methods. Therefore, the design for better defense mechanisms to improve the robustness of deep neural networks is a vital challenge that urgently needs to be addressed.

#### 4.6. Ablation Study on Hyper-parameters

In this section, we conduct a series of ablation experiments on the hyperparameters. We consider Inc-v3 to generate adversarial examples under the CT method and transfer them to all models, and then do separate ablation experiments on pre-convergences as well as the search amplification factor. All experimental hyperparameters of the other methods are kept constant.

**Pre-convergence Iterations  $P$ .** Given the sequential necessity of both pre-convergence and global search, we first explore the effect of pre-convergence rounds  $p$  on the attack results. As the experimental results in Figure 4a, 4b demonstrate, we can find that just one step of pre-convergence yields a certain performance improvement that increases gradually with incremental  $P$  until it stabilizes. This is a strong indication that there is gradient elimination in the unpreconverged gradient, and that pre-convergence suppresses this phenomenon, thus improving attack performance. Finally, we choose  $P = 5$  to balance the success rate of the attack with the time taken by the attack.

**Global Search Factor  $S$ .** After determining the number of pre-convergence iterations, we further investigate the effect of the global search factor at  $P = 5$ , the results are shown in Figure 4c. It can be seen that the attack performance improves significantly with the increase of the amplification factor and gradually stabilizes, which illustrates that the global search helps the momentum to find a better global optimal solution. In the end, we choose  $S = 10$ .

### 5. Conclusion

In this paper, from the perspective of gradient cosine consistency, we first analyse and identify the shortcomings of existing optimization methods, namely gradient elimination, which can lead to unsatisfactory forward attack attempts. At the same time, traditional iterative attacks adopt smaller steps to restrict the attack to optimize within a smaller data distribution, resulting in an attack that tends to fall into a local optimum. Our proposal is to address these issues by global momentum initialization in the form of high-step size pre-convergence, which provides a high-quality direction for the attack during the initial stage, suppressing gradient elimination and enhancing its performance significantly. Our approach can be combined with almost all gradient-based optimization methods. Empirical experiments demonstrate that our method achieves an average success rate of 95.4% with the nine existing advanced defense methods, significantly exceeding the previous state-of-the-art success rate of 89%. We hope our method can be served as a new baseline to validate the effectiveness of existing defense methods in the future.

**Broader impacts.** In this work, we propose global momentum initialization to significantly improve transfer



attack performance under black-box setting, further highlighting the potential for practical adversarial attacks and the vulnerability of existing DNNs. We hope to shed insight on ways to improve the robustness of neural networks from an attack perspective in order to build more effective and secure DNNs.

## References

- [1] Mariusz Bojarski, Davide Del Testa, Daniel Dworakowski, Bernhard Firner, Beat Flepp, Prasoon Goyal, Lawrence D Jackel, Mathew Monfort, Urs Muller, Jiakai Zhang, et al. End to end learning for self-driving cars. *arXiv preprint arXiv:1604.07316*, 2016.
- [2] Nicholas Carlini and David Wagner. Towards evaluating the robustness of neural networks. In *2017 IEEE Symposium on Security and Privacy (SP)*, pages 39–57. Ieee, 2017.
- [3] Zhaoyu Chen, Bo Li, Shuang Wu, Shouhong Ding, and Wenqiang Zhang. Query-efficient decision-based black-box patch attack. *arXiv preprint arXiv:2307.00477*, 2023.
- [4] Zhaoyu Chen, Bo Li, Shuang Wu, Kaixun Jiang, Shouhong Ding, and Wenqiang Zhang. Content-based unrestricted adversarial attack. *arXiv preprint arXiv:2305.10665*, 2023.
- [5] Zhaoyu Chen, Bo Li, Shuang Wu, Jianghe Xu, Shouhong Ding, and Wenqiang Zhang. Shape matters: deformable patch attack. In *European Conference on Computer Vision*, pages 529–548. Springer, 2022.
- [6] Zhaoyu Chen, Bo Li, Jianghe Xu, Shuang Wu, Shouhong Ding, and Wenqiang Zhang. Towards practical certifiable patch defense with vision transformer. In *Proceedings of the IEEE/CVF Conference on Computer Vision and Pattern Recognition*, pages 15148–15158, 2022.
- [7] Jeremy M. Cohen, Elan Rosenfeld, and J. Zico Kolter. Certified adversarial robustness via randomized smoothing. In Kamalika Chaudhuri and Ruslan Salakhutdinov, editors, *Proceedings of the 36th International Conference on Machine Learning, ICML 2019, 9-15 June 2019, Long Beach, California, USA*, volume 97 of *Proceedings of Machine Learning Research*, pages 1310–1320. PMLR, 2019.
- [8] Yinpeng Dong, Fangzhou Liao, Tianyu Pang, Xiaolin Hu, and Jun Zhu. Discovering adversarial examples with momentum. *arXiv preprint arXiv:1710.06081*, 2017.
- [9] Yinpeng Dong, Tianyu Pang, Hang Su, and Jun Zhu. Evading defenses to transferable adversarial examples by translation-invariant attacks. In *Proceedings of the IEEE/CVF Conference on Computer Vision and Pattern Recognition*, pages 4312–4321, 2019.
- [10] Lianli Gao, Qilong Zhang, Jingkuan Song, Xianglong Liu, and Heng Tao Shen. Patch-wise attack for fooling deep neural network. In *European Conference on Computer Vision*, pages 307–322. Springer, 2020.
- [11] Ian J. Goodfellow, Jonathon Shlens, and Christian Szegedy. Explaining and harnessing adversarial examples. In *ICLR*, 2015.
- [12] Chuan Guo, Mayank Rana, Moustapha Cisse, and Laurens Van Der Maaten. Countering adversarial images using input transformations. *arXiv preprint arXiv:1711.00117*, 2017.
- [13] Pinxue Guo, Wei Zhang, Xiaoqiang Li, and Wenqiang Zhang. Adaptive online mutual learning bi-decoders for video object segmentation. *IEEE Transactions on Image Processing*, 2022.
- [14] Kaiming He, Xiangyu Zhang, Shaoqing Ren, and Jian Sun. Deep residual learning for image recognition. In *Proceedings of the IEEE conference on computer vision and pattern recognition*, pages 770–778, 2016.
- [15] Kaiming He, Xiangyu Zhang, Shaoqing Ren, and Jian Sun. Identity mappings in deep residual networks. In Bastian Leibe, Jiri Matas, Nicu Sebe, and Max Welling, editors, *Computer Vision - ECCV 2016 - 14th European Conference, Amsterdam, The Netherlands, October 11-14, 2016, Proceedings, Part IV*, volume 9908 of *Lecture Notes in Computer Science*, pages 630–645. Springer, 2016.
- [16] Lingyi Hong, Wenchao Chen, Zhongying Liu, Wei Zhang, Pinxue Guo, Zhaoyu Chen, and Wenqiang Zhang. Lvos: A benchmark for long-term video object segmentation, 2022.
- [17] Lingyi Hong, Wei Zhang, Liangyu Chen, Wenqiang Zhang, and Jianping Fan. Adaptive selection of reference frames for video object segmentation. *IEEE Transactions on Image Processing*, 31:1057–1071, 2022.
- [18] Hao Huang, Ziyang Chen, Huanran Chen, Yongtao Wang, and Kevin Zhang. T-sea: Transfer-based self-ensemble attack on object detection. In *Proceedings of the IEEE/CVF Conference on Computer Vision and Pattern Recognition*, pages 20514–20523, 2023.
- [19] Hao Huang, Yongtao Wang, Zhaoyu Chen, Zhi Tang, Wenqiang Zhang, and Kai-Kuang Ma. Rpattack: Refined patch attack on general object detectors. In *2021 IEEE International Conference on Multimedia and Expo (ICME)*, pages 1–6. IEEE, 2021.
- [20] Hao Huang, Yongtao Wang, Zhaoyu Chen, Yuze Zhang, Yuheng Li, Zhi Tang, Wei Chu, Jingdong Chen, Weisi Lin, and Kai-Kuang Ma. Cmu-watermark: A cross-model universal adversarial watermark for combating deepfakes. In *Proceedings of the AAAI Conference on Artificial Intelligence*, volume 36, pages 989–997, 2022.
- [21] Tony Huang, Jack Chu, and Fangyun Wei. Unsupervised prompt learning for vision-language models. *arXiv preprint arXiv:2204.03649*, 2022.
- [22] Xiaojun Jia, Xingxing Wei, Xiaochun Cao, and Hassan Foroosh. Comdefend: An efficient image compression model to defend adversarial examples. In *IEEE Conference on Computer Vision and Pattern Recognition, CVPR 2019, Long Beach, CA, USA, June 16-20, 2019*, pages 6084–6092. Computer Vision Foundation / IEEE, 2019.
- [23] Kaixun Jiang, Zhaoyu Chen, Tony Huang, Jiafeng Wang, Dingkan Yang, Bo Li, Yan Wang, and Wenqiang Zhang. Efficient decision-based black-box patch attacks on video recognition. *arXiv preprint arXiv:2303.11917*, 2023.
- [24] Alexey Kurakin, Ian J Goodfellow, and Samy Bengio. Adversarial examples in the physical world. In *Artificial intelligence safety and security*, pages 99–112. Chapman and Hall/CRC, 2018.
- [25] Xiangpeng Li, Lianli Gao, Xuanhan Wang, Wu Liu, Xing Xu, Heng Tao Shen, and Jingkuan Song. Learnable aggregating net with diversity learning for video question answering.

- In *Proceedings of the 27th ACM international conference on multimedia*, pages 1166–1174, 2019.
- [26] Fangzhou Liao, Ming Liang, Yinpeng Dong, Tianyu Pang, Xiaolin Hu, and Jun Zhu. Defense against adversarial attacks using high-level representation guided denoiser. In *2018 IEEE Conference on Computer Vision and Pattern Recognition, CVPR 2018, Salt Lake City, UT, USA, June 18-22, 2018*, pages 1778–1787. Computer Vision Foundation / IEEE Computer Society, 2018.
  - [27] Jiadong Lin, Chuanbiao Song, Kun He, Liwei Wang, and John E. Hopcroft. Nesterov accelerated gradient and scale invariance for improving transferability of adversarial examples. *CoRR*, abs/1908.06281, 2019.
  - [28] Siao Liu, Zhaoyu Chen, Wei Li, Jiwei Zhu, Jiafeng Wang, Wenqiang Zhang, and Zhongxue Gan. Efficient universal shuffle attack for visual object tracking. In *ICASSP 2022-2022 IEEE International Conference on Acoustics, Speech and Signal Processing (ICASSP)*, pages 2739–2743. IEEE, 2022.
  - [29] Yanpei Liu, Xinyun Chen, Chang Liu, and Dawn Song. Delving into transferable adversarial examples and black-box attacks. In *5th International Conference on Learning Representations, ICLR 2017, Toulon, France, April 24-26, 2017, Conference Track Proceedings*. OpenReview.net, 2017.
  - [30] Yang Liu, Jing Liu, Wei Ni, and Liang Song. Abnormal event detection with self-guiding multi-instance ranking framework. In *2022 International Joint Conference on Neural Networks (IJCNN)*, pages 01–07, 2022.
  - [31] Yang Liu, Jing Liu, Mengyang Zhao, Dingkan Yang, Xiaoguang Zhu, and Liang Song. Learning appearance-motion normality for video anomaly detection. In *2022 IEEE International Conference on Multimedia and Expo (ICME)*, pages 1–6, 2022.
  - [32] Yang Liu, Jing Liu, Xiaoguang Zhu, Donglai Wei, Xiaohong Huang, and Liang Song. Learning task-specific representation for video anomaly detection with spatial-temporal attention. In *ICASSP 2022 - 2022 IEEE International Conference on Acoustics, Speech and Signal Processing (ICASSP)*, pages 2190–2194, 2022.
  - [33] Zihao Liu, Qi Liu, Tao Liu, Nuo Xu, Xue Lin, Yanzhi Wang, and Wujie Wen. Feature distillation: Dnn-oriented jpeg compression against adversarial examples. In *2019 IEEE/CVF Conference on Computer Vision and Pattern Recognition (CVPR)*, pages 860–868. IEEE, 2019.
  - [34] Muzammal Naseer, Salman H. Khan, Munawar Hayat, Fahad Shahbaz Khan, and Fatih Porikli. A self-supervised approach for adversarial robustness. In *2020 IEEE/CVF Conference on Computer Vision and Pattern Recognition, CVPR 2020, Seattle, WA, USA, June 13-19, 2020*, pages 259–268. Computer Vision Foundation / IEEE, 2020.
  - [35] Yuri Nesterov. A method for unconstrained convex minimization problem with the rate of convergence  $O(1/k^2)$ . In *Doklady an ussr*, volume 269, pages 543–547, 1983.
  - [36] Nicolas Papernot, Patrick D. McDaniel, Ian J. Goodfellow, Somesh Jha, Z. Berkay Celik, and Ananthram Swami. Practical black-box attacks against deep learning systems using adversarial examples. *CoRR*, abs/1602.02697, 2016.
  - [37] Nicolas Papernot, Patrick D. McDaniel, Ian J. Goodfellow, Somesh Jha, Z. Berkay Celik, and Ananthram Swami. Practical black-box attacks against machine learning. In Ramesh Karri, Ozgur Sinanoglu, Ahmad-Reza Sadeghi, and Xun Yi, editors, *Proceedings of the 2017 ACM on Asia Conference on Computer and Communications Security, AsiaCCS 2017, Abu Dhabi, United Arab Emirates, April 2-6, 2017*, pages 506–519. ACM, 2017.
  - [38] Olga Russakovsky, Jia Deng, Hao Su, Jonathan Krause, Sanjeev Satheesh, Sean Ma, Zhiheng Huang, Andrej Karpathy, Aditya Khosla, Michael S. Bernstein, Alexander C. Berg, and Fei-Fei Li. Imagenet large scale visual recognition challenge. *Int. J. Comput. Vis.*, 115(3):211–252, 2015.
  - [39] Christian Szegedy, Sergey Ioffe, Vincent Vanhoucke, and Alexander A Alemi. Inception-v4, inception-resnet and the impact of residual connections on learning. In *Thirty-first AAAI conference on artificial intelligence*, 2017.
  - [40] Christian Szegedy, Vincent Vanhoucke, Sergey Ioffe, Jonathon Shlens, and Zbigniew Wojna. Rethinking the inception architecture for computer vision. In *CVPR*, pages 2818–2826, 2016.
  - [41] Christian Szegedy, Wojciech Zaremba, Ilya Sutskever, Joan Bruna, Dumitru Erhan, Ian J. Goodfellow, and Rob Fergus. Intriguing properties of neural networks. In Yoshua Bengio and Yann LeCun, editors, *ICLR*, 2014.
  - [42] Florian Tramèr, Alexey Kurakin, Nicolas Papernot, Ian J. Goodfellow, Dan Boneh, and Patrick D. McDaniel. Ensemble adversarial training: Attacks and defenses. In *International Conference on Learning Representations*, 2018.
  - [43] Hao Wang, Yitong Wang, Zheng Zhou, Xing Ji, Dihong Gong, Jingchao Zhou, Zhifeng Li, and Wei Liu. Cosface: Large margin cosine loss for deep face recognition. In *Proceedings of the IEEE conference on computer vision and pattern recognition*, pages 5265–5274, 2018.
  - [44] Xiaosen Wang and Kun He. Enhancing the transferability of adversarial attacks through variance tuning. In *IEEE Conference on Computer Vision and Pattern Recognition, CVPR 2021, virtual, June 19-25, 2021*, pages 1924–1933. Computer Vision Foundation / IEEE, 2021.
  - [45] Xiaosen Wang, Xuanran He, Jingdong Wang, and Kun He. Admix: Enhancing the transferability of adversarial attacks. In *Proceedings of the IEEE/CVF International Conference on Computer Vision*, pages 16158–16167, 2021.
  - [46] Yuzheng Wang, Zhaoyu Chen, Dingkan Yang, Yang Liu, Siao Liu, Wenqiang Zhang, and Lizhe Qi. Adversarial contrastive distillation with adaptive denoising. In *ICASSP 2023-2023 IEEE International Conference on Acoustics, Speech and Signal Processing (ICASSP)*, pages 1–5. IEEE, 2023.
  - [47] Cihang Xie, Jianyu Wang, Zhishuai Zhang, Zhou Ren, and Alan Yuille. Mitigating adversarial effects through randomization. *arXiv preprint arXiv:1711.01991*, 2017.
  - [48] Cihang Xie, Zhishuai Zhang, Yuyin Zhou, Song Bai, Jianyu Wang, Zhou Ren, and Alan L Yuille. Improving transferability of adversarial examples with input diversity. In *Proceedings of the IEEE/CVF Conference on Computer Vision and Pattern Recognition*, pages 2730–2739, 2019.

- [49] Weilin Xu, David Evans, and Yanjun Qi. Feature squeezing: Detecting adversarial examples in deep neural networks. In *25th Annual Network and Distributed System Security Symposium, NDSS 2018, San Diego, California, USA, February 18-21, 2018*. The Internet Society, 2018.
- [50] Dingkang Yang, Zhaoyu Chen, Yuzheng Wang, Shunli Wang, Mingcheng Li, Siao Liu, Xiao Zhao, Shuai Huang, Zhiyan Dong, Peng Zhai, and Lihua Zhang. Context de-confounded emotion recognition. In *Proceedings of the IEEE/CVF Conference on Computer Vision and Pattern Recognition (CVPR)*, pages 19005–19015, June 2023.
- [51] Dingkang Yang, Shuai Huang, Haopeng Kuang, Yangtao Du, and Lihua Zhang. Disentangled representation learning for multimodal emotion recognition. In *Proceedings of the 30th ACM International Conference on Multimedia*, page 1642–1651, 2022.
- [52] Dingkang Yang, Shuai Huang, Shunli Wang, Yang Liu, Peng Zhai, Liuzhen Su, Mingcheng Li, and Lihua Zhang. Emotion recognition for multiple context awareness. In *Proceedings of the European Conference on Computer Vision*, volume 13697, pages 144–162. Springer, 2022.
- [53] Dingkang Yang, Shuai Huang, Zhi Xu, Zhenpeng Li, Shunli Wang, Mingcheng Li, Yuzheng Wang, Yang Liu, Kun Yang, Zhaoyu Chen, et al. Aide: A vision-driven multi-view, multimodal, multi-tasking dataset for assistive driving perception. *arXiv preprint arXiv:2307.13933*, 2023.
- [54] Dingkang Yang, Haopeng Kuang, Shuai Huang, and Lihua Zhang. Learning modality-specific and -agnostic representations for asynchronous multimodal language sequences. In *Proceedings of the 30th ACM International Conference on Multimedia*, page 1708–1717, 2022.
- [55] Dingkang Yang, Yang Liu, Can Huang, Mingcheng Li, Xiao Zhao, Yuzheng Wang, Kun Yang, Yan Wang, Peng Zhai, and Lihua Zhang. Target and source modality co-reinforcement for emotion understanding from asynchronous multimodal sequences. *Knowledge-Based Systems*, 265:110370, 2023.
- [56] Jie Zhang, Bo Li, Jianghe Xu, Shuang Wu, Shouhong Ding, Lei Zhang, and Chao Wu. Towards efficient data free black-box adversarial attack. In *Proceedings of the IEEE/CVF Conference on Computer Vision and Pattern Recognition*, pages 15115–15125, 2022.
- [57] Jie Zhang, Lei Zhang, Gang Li, and Chao Wu. Adversarial examples for good: Adversarial examples guided imbalanced learning. *arXiv preprint arXiv:2201.12356*, 2022.